Investigation of spiral blood flow in a model of arterial stenosis

Manosh C Paul* and Arkaitz Larman

Department of Mechanical Engineering, University of Glasgow, Glasgow, G12 8QQ, UK

*Corresponding author: Email:m.paul@mech.gla.ac.uk, Tel: +44 (0)141 330 8466,

Fax: +44 (0)141 330 4343

Abstract:

The spiral component of blood flow has both beneficial and detrimental effects in human circulatory system (Stonebridge and Brophy [1]). We investigate the effects of the spiral blood flow in a model of three-dimensional arterial stenosis with a 75% cross-sectional area reduction at the centre by means of computational fluid dynamics (CFD) techniques. The standard k-ω model is employed for simulation of the blood flow for the Reynolds number of 500 and 1000. We find that for Re=500 the spiral component of the blood flow increases both the total pressure and velocity of the blood, and some significant differences are found between the wall shear stresses of the spiral and non-spiral induced flow downstream of the stenosis. The turbulent kinetic energy is reduced by the spiral flow as it induces the rotational stabilities in the forward flow. For Re=1000 the tangential component of the blood velocity is most influenced by the spiral speed, but the effect of the spiral flow on the centreline turbulent kinetic energy and shear stress is mild. The results of the effects of the spiral flow are discussed in the paper along with the relevant pathological issues.

1 Introduction

The hemodynamics in blood vessels of human circulatory system is often associated with the pathophysiology of cardiovascular diseases. Therefore, a thorough understanding of blood dynamics in human vessels is of great interest, as it is well known that the flow pattern interacts directly with the vessel walls and, thus, can cause both beneficial and detrimental effect on its endothelium (type of cells that cover blood vessels) walls (Friedman et al. [2] and Ku et al [3]). A deep knowledge of blood-flow patterns is essential to identify relationships between the patterns and the diseases that form on arteries and vein branches, therefore, the study of physiological blood flow is quite important and nowadays the computational simulation is playing a significant role in this field.

Numerous computational and experimental studies have been performed to model and investigate the blood flow in arterial stenosis, see the papers of Ahmed and Giddens [4], Ghalichi et al. [5], Lee et al. [6], Paul et al. [7] and Sarifuddin et al. [8], and the relevant references therein. In [4] the effects of various percentages of axisymmetric stenosis on the velocity field in the post-stenosis zone were investigated by using laser Doppler anemometry and flow visualisation techniques. In the experiment, the flow at the upstream was kept steady and the Reynolds numbers within the range of 500 to 2000 were considered in the study. The k-ω turbulent model was applied by Ghalichi et al. [5] to study the blood flow in the same stenosed model of artery as in [4]. Their results show that the k-ω model performs better than the standard k-ε model in terms of predicting the pressure and turbulence intensity of the blood flow. The results presented in Lee et al. [6], who investigated the turbulent flow through a series of axisymmetric stenosis by imposing a steady parabolic profile at the upstream, also suggest that the k-ω model is good enough in the prediction of the laminar as

well as turbulent flow in the stenosed vessel. However, the limitation of the k-ω model in the modelling of transient blood flow through the stenosis is highlighted in Paul et al. [7] who used the Large Eddy Simulation technique in their model. The smooth constriction, which was generated using the cosine relation of [4], gives a fairly accurate representation of an arterial stenosis. But the recent numerical paper of Sarifuddin et al. [8] shows that the post-stenotic results are largely influenced by the choice of the stenosis used in the model. Three different shapes of the stenosis such as cosine form, irregular shape and smooth are considered in [8] and the blood flow through them is investigated numerically prescribing a parabolic profile of the streamwise velocity at the inlet.

It is evident from the in-vivo research of Stonebridge and Brophy [1] and Stonebridge et al. [9] that the blood flow through artery is spiral type because of the twisting of heart on its own axis. So the previous in-vitro models [4-8] do not represent truly the blood flow patterns at the inlet of artery. This spiral component of blood velocity can have both beneficial and detrimental effects according to Stonebridge and Brophy [1]. Even though all these effects are not yet well understood, it is sure that the spiral component in the blood flow has to be studied for better comprehension of the blood flow in the circulatory system. Moreover, Stonebridge et al. [10] concluded that the spiral blood flow can not only reduce the laterally directed forces and turbulence caused by stenosis but also induce stability over non-spiral flow that prevents disturbance of normal blood flow pattern in a stenosed vessel. To the authors' knowledge, this is the only published paper [10] which looked into the non-spiral and spiral flows in stenosis by using magnetic resonance imagining (MRI) and computational fluid dynamics (CFD, Star-CD commercial package). A constant streamwise velocity with a rotational speed (1/6th of the streamwise velocity) was used at the inlet of the model and the effect of spiral flow was investigated. However, the effects of the variations of the flow velocity (i.e. Reynolds

number) along with the variation of the spiral speed on the results of the transient blood flow downstream of the stenosis have not been investigated by them.

In the present paper, our aim is to investigate the spiral blood flow in a model of stenosed artery with 75% constriction by means of computational fluid dynamics (CFD) techniques. In particular, we focus on how the spiral nature of the flow profile, that is prescribed along with the parabolic streamwise velocity at the inlet of the model, affects the important results such as blood pressure, velocity, wall shear stresses and turbulence at the downstream of the stenosis. In the simulation, the standard k-ω model of Wilcox [11] is employed for the Reynolds number of 500 and 1000. The formulations of the model with boundary conditions and the numerical techniques used are summarised in Sections 2 and 3 respectively. This is followed by the results and discussion in Section 4, and a general conclusion of the work is drawn in Section 5.

2 Problem formulations

The stenosis in the blood vessel shown in Fig. 1(a) is created using the following cosine-form formula [4],

$$\frac{r(Z)}{R} = 1 - \delta_c \left[1 + \cos\left(\frac{Z\pi}{D}\right) \right], \quad -D \leq Z \leq D \tag{1}$$

where R and D are the radius and diameter of the unstenosed vessel respectively; and r and Z are the radial and axial coordinates. The parameter, δ_c, that controls the percentage of the stenosis is fixed to 0.25, giving a 75% reduction of the cross-sectional area at the centre of the stenosis. The smooth reduction of the cross-sectional area generated inside the vessel using the relation (1) provides a fairly accurate representation of a biological form of arterial stenosis [4]. The total length of model is taken as 540mm (27D) where diameter D=20mm

[4]. The length of the stenosed zone is 2D=40mm, and 21D and 4D are the downstream and upstream length respectively from the stenosis. In Fig. 1(b), the spiral boundary condition along with the parabolic flow used at the inlet of the model is illustrated.

We assume that the blood flow through the model is incompressible and the blood is a Newtonian and homogeneous fluid ([12]) with a density of ρ=1060 kg/m^3 and a constant dynamic viscosity of μ=3.71·10^{-3} Pa·s. The governing equations of motion of the blood flow are considered as the Navier-Stokes equations, and after applying the Reynolds time-averaging techniques, the Reynolds-averaged Navier-Stokes (RANS) are obtained and written in the tensor form as [13],

$$\frac{\partial u_i}{\partial x_i} = 0 \qquad\qquad [2]$$

$$\frac{\partial}{\partial t}\left(\rho u_i\right) + \frac{\partial}{\partial x_j}\left(\rho u_i u_j\right) = -\frac{\partial p}{\partial x_i} + \frac{\partial}{\partial x_j}\left[\mu\left(\frac{\partial u_i}{\partial x_j} + \frac{\partial u_j}{\partial x_i}\right)\right] + \frac{\partial \tau_{ij}}{\partial x_j} \qquad\qquad [3]$$

where u_i are the mean velocity components along the Cartesian co-ordinate systems, x_i=(x, y, z), p is the pressure and τ_{ij} are the Reynolds stresses which are modelled employing the Boussinesq hypothesis as

$$\tau_{ij} = -\rho\left\langle u_i' u_j'\right\rangle = \mu_t\left(\frac{\partial u_i}{\partial x_j} + \frac{\partial u_j}{\partial x_i}\right) - \frac{2}{3}\rho k \delta_{ij} \qquad\qquad [4]$$

where u_i' are the fluctuating velocity components; $k = \frac{1}{2}\left\langle u_i' u_i'\right\rangle$ is the turbulent kinetic energy and μ_t is the turbulent viscosity obtained by employing the standard k-ω model of Wilcox [11]. The details of this turbulent model can be found in [11, 13].

5

The blood vessel of artery has been simplified in the model considering it as a rigid and impermeable circular tube with a no-slip boundary condition for fluid having zero velocity ($u_i = 0$) relative to the boundary. A parabolic profile of the streamwise component of the three-dimensional velocity,

$$\text{v}(x, y) = 2V \left[1 - \left(\frac{r}{R} \right)^2 \right],$$
[5]

where V is the bulk streamwise velocity related to the Reynolds number, $\text{Re} = \rho V D / \mu$, of the blood flow, has been imposed at the inlet of the model; and to investigate the effects of the spiral laminar flow in the stenosed vessel a number of different spiral or rotational velocities have been applied. The spiral velocity (Ω) has been defined as a fraction of the forward velocity within the vessel, which has been calculated using the following relation:

$$\Omega = \frac{V}{R} C$$
[6]

where C is a constant that controls the magnitude of the spiral speed. The value of the constant C in real blood flow usually takes $\frac{1}{6}$ as mentioned in [10, 11]. However, in the computation, we have used some other values of C which are higher or lower than $\frac{1}{6}$ in order to compare the results at the different spiral velocities. Table 1 shows the values of the spiral speed for Re=500 and 1000 obtained by using the different values of C and applied in the simulation. In addition, the outlet of the model has been treated as a pressure outlet using the default setting for the gauge pressure to become zero at the outlet, Fluent [13].

3 Overview of the numerical methods

Fluent [13] uses the finite volume method to discretise the governing equations (2, 3) forming a system of algebraic equations which has been solved by using an iterative process. The SIMPLE method of Patankar [14] is triggered to couple the velocity with pressure. In the discretisation process, the second order upwind scheme is used for the equations of momentum, turbulent kinetic energy (k) and specific dissipation rate (ω); while the second order accurate scheme is used for the Poisson-like pressure equation.

The pressure based implicit solver is chosen to solve the discretised algebraic equations keeping the absolute formulation for the velocity. The default values for the under relaxation factors for the pressure, momentum and k-ω equations are used in the solution process, details of these can be found in the documents of Fluent [13]. The inlet boundary conditions for the streamwise velocity and the spiral speed are written in C-language using the interface of User Defined Function (UDF) of Fluent and linked with the solver.

The solution process is initiated using arbitrary values of the velocity components and k-ω, and their residuals are monitored at every iteration. The magnitude of the residuals dropped gradually, which is a strong indicator for the stable and accurate solutions, and the iteration process is stopped when the residuals are levelled off at 10^{-6} (in fact the residuals became independent to the iteration number at this level) and the final converged solutions are achieved.

4 Results and discussion

A grid independence test has been performed to ensure that the numerical solutions are independent on the choice of the grid arrangements. The results of this test are presented in Figs. 2 and 3 for the axial velocity profiles at the different positions along the flow. The Reynolds number in Fig.2 is taken as Re=500 with the spiral speed of Ω=1.46 rad/sec, while in Fig.2 Re is 1000 with Ω=2.92 rad/sec. Initially, for Grid 1 the computational domain was discretised into a total of 718,627 control volumes, which was then increased by about 25% for Grid 2 consisting of a total of 891,131 control volumes. A further increment of over 110% was made for Grid 3 which consists of a massive 1,925,160 control volumes in the whole computational domain. The results in Figs. 2 and 3 clearly demonstrate that the resolution of Grid 1 for the numerical solutions is good enough for both the Reynolds numbers under consideration.

Fig. 4 shows the effects of the spiral flow on the total pressure at the centre of the model artery. For Re=500 the total pressure increases at the downstream of the stenosis with the swirl velocity, which can clearly be seen in the downstream region between 0.1m and 0.2m. However, at the immediate downstream of the stenosis and towards the far downstream the effects of the spiral flow is quite mild, and for Re=1000 almost no variation in the centreline total pressure is observed in frame (b). The corresponding velocity profiles, presented in Fig. 5, show that the tangential component of the velocity is largely affected by the spiral flow for both Re=500 and 1000, causing a gradual rise in the tangential velocity as the spiral speed (Ω) increases. No substantial effect of the spiral flow on the radial and axial components of the velocity is found for Re=1000, but the results for Re=500 show some levels of variation in the radial and axial velocities at the centre. In particular, the axial velocity increases with the

spiral speed within the downstream region between 0.1m and 0.2m, while the peak in the radial velocity drops as Ω increases. The contour plot in Fig. 6 provides further information on how the magnitude of the tangential velocity in the mid-plane of the stenosed artery is affected by the spiral speed. As the spiral speed increases, the tangential velocity at the downstream of the stenosis increases, and particularly, the effect is higher for Re=1000 compared to Re=500.

The wall shear stresses, which were recorded at the four different phases for Re=500, have been presented in Fig. 7 to show how they are influenced by the spiral flow. Note that in order to get the phases two perpendicular planes along the model's x and y axes were first defined and the shear stresses at the four intersected points of these two planes with the arterial wall were then calculated, a schematic showing the phases is given in Fig. 7. Some interesting but rather complex patterns of the shear stress are predicted in the wall due to the spiral effect on the blood flow, and clearly the two large peaks, which are found at the downstream of the stenosis, depend on both the spiral speeds and the phases. For example, in the second peak the maximum value occurs at phase 2 for Ω=0.73 rad/s (frame a), while the maximum is recorded at phase 3 (frames b-d) for higher spiral speeds. On the other hand, the maximum value of the first peak occurring at phase 4 for Ω=0.73 rad/s (frame a) remains persistent for all the other values of Ω. Although phases 1 and 3 try to catch up the maximum level of phase 4, surprisingly the growth of the first peak at phase 2 falls down sharply for Ω=1.46 rad/s, 2.19 rad/s and 2.92 rad/s (frames b to d).

In addition, the comparisons of the results of the wall shear stress between the non-spiral for which Ω=0 and the various spiral speeds show some distinct features at the downstream of the stenosis particularly within the region of $0 < Z(m) < 0.25$. The second peak at phases 2 and 3

for the spiral flow is always greater than the non-spiral case, while it is slightly lower at phases 1 and 4. On the other hand, the first peak at phases 1, 3 and 4 for the spiral speed higher than 0.73 rad/s is always greater than the non-spiral case, and at phase 2 it is significantly lower. However, towards the further downstream as the spiral effect found on the velocity field is less prominent, the wall shear stress eventually stabilises into a constant value. Fig. 8 also reports that the spiral effects on the wall shear stress for Re=1000 are mild and the pattern is very similar to that of the non-spiral flow.

The effect of the spiral speeds on the separated blood flow from the throat of the stenosis is more clearly visible in Fig 9, where the pathlines, coloured by the particle ID, are plotted for the different spiral speeds whilst Re=500. The recirculation region and the structure of the blood flow downstream of the stenosis are affected by the spiral flow, producing twisted three-dimensional flow situated at the downstream of the stenosis, and the pattern of this flow is similar to that of the MRI measurement of the blood flow in a patient's artery with thrombosis done by Frydrychowicz et al. [15]. They also termed the pattern of this twisting flow as "corkscrew". In order to see the effects more clearly, cross-sectional views of the flow streamlines are presented in Fig. 10 for Ω=1.46 rad/s. The intensity of the twisting flow at about 5D-distance downstream of the throat of the stenosis is quite strong and the flow pattern is much chaotic than that seen in the further downstream region. In the pathological context, these strong circulations in the post-stenotic blood flow usually influence to cause potential damage to blood cells and inner surface of the stenosed artery.

In the final figure, Fig. 11, we examine the effects of the spiral flow on the turbulence downstream of the stenosis. The production of the turbulent kinetic energy (k) for Re=500 is reduced with the increment of the spiral speed because the spiral laminar flow, which was

prescribed at the inlet on the model, induces rotational stability of the forward blood flow downstream of the stenosis, Stonebridge et al. [10]. For the non-spiral flow, the result shows that the turbulence is over-predicted in the model, however, for Re=1000 no variation in the centreline turbulent kinetic energy found with the spiral flow as already reported in Fig. 5 that the streamwise velocity whose magnitude is much higher than the radial and tangential velocities is not largely affected by the spiral speed in this case. In order to get a significant effect of the spiral flow for Re=1000, one needs to increase the spiral speed at the inlet which may not be physiologically realistic.

5 Conclusion

The standard k-ω turbulent model is employed to investigate the effects of the spiral laminar blood flow through the model of a 75% stenosed artery. The "corkscrew" type flow patterns are observed at the downstream of the stenosis due to the spiral flow. For Re=500 the spiral flow increases the total pressure and velocity of the blood, and significant differences are found between the wall shear stresses of the spiral and non-spiral induced flows downstream of the stenosis. The results also show that the turbulent kinetic energy is reduced by the spiral flow as it induces the rotational stabilities in the forward flow. While for Re=1000, no significant difference is found in the centreline turbulent kinetic energy between the spiral and non-spiral flows and the effect is mild on the centreline shear stresses. However, the tangential component of the velocity is most influenced by the spiral flow and it is increased when the spiral speed increases.

As already mentioned, the spiral component of blood flow has both beneficial and detrimental effects in human circulatory system [1]. The results of the effects of the spiral blood flow through the stenosis, which are presented in the paper, are of great interest in the pathological context and have relevant clinical significances. For example, the rise of the turbulent kinetic energy in the post-stenotic region is responsible to cause damage to the blood-cell materials and to activate platelets in the blood, and subsequently, they create many pathological diseases (Ku [12]). However, the results show that the spiral effect reduces the turbulent kinetic energy, which is a beneficial effect; but at the same time it produces oscillating wall shear stress in the post stenosis, which is a detrimental effect as the oscillating shear stress usually influence to cause potential damage to the inner side of a post-stenotic blood vessel, kwon as endothelium (Fry [16]). In addition, the strong circulation seen in the post-stenosis due to the spiral effect is harmful as it can cause the blood to be clotted in the post-stenosis, which is a potential source of stroke.

The model studied in the paper is simplified by considering a rigid wall for the vessels. The future extension of this paper is to couple the spiral blood flow with the deformation of the arterial wall, which will certainly involve some significant challenges in simulation. As the spiral flow has potential clinical significance, therefore, we believe that this paper will have some significant impacts on the understanding of blood flow dynamics and its relevance in arterial diseases such as stenosed artery.

References

1. Stonebridge, P.A., BROPHY, C.M., Spiral laminar flow in arteries?, The Lancet, 338, 1360-1361, 1991.

2. Friedman, M.H., Hutchins, G.M., Bargeron, C.B., Deters, O.J., Mark, F.F., Correlation between intimal thickness and fluid shear in human arteries, Atherosclerosis, 39, 425-436, 1981.

3. Ku, D.N., Giddens, D.P., Zarins, C.K., Glagov, S., Pulsatile flow and atherosclerosis in the human carotid bifurcation. Positive correlation between plaque location and low oscillating shear stress, Atherosclerosis, 5, 293-302, 1985.

4. Ahmed, S.A., Giddens, D.P., Velocity measurements in steady flow through axisymmetric stenoses at moderate Reynolds number. J. Biomechanics, 16, 505-516, 1983.

5. Ghalichi, F., Deng, X, Champlan, A., Douville, Y. King, M., Guidoin, R, Low Reynolds number turbulence modelling of blood flow in arterial stenosis, Biorheology, 35, 281-284, 1998.

6. Lee, T.S., Liao, W., Low, H.T., Numerical simulation of turbulent flow through series stenoses. Int. J. Numerical Methods in Fluids, 42, 717–740, 2003.

7. Paul, M.C., Molla, M.M., Roditi, G., Large–Eddy simulation of pulsatile blood flow, Medical Engineering & Physics, 31, 153–159, 2009.

8. Sarifuddin, Chakravarty, S., Mandal, P.K, Layek, G.C., Numerical simulation of unsteady generalized Newtonian blood flow through differently shaped distensible arterial stenoses, J. Medical Engineering & Technology, 32, 385-399, 2008.

9. Stonebridge, P.A., Hoskins, P.R., Allan, P.L., Belch, F.F., Spiral laminar flow in vivo, Clinical Science, 91, 17-21, 1996.

10. Stonebridge, P.A., Buckley, C., Thompson, A., Dick, J., Hunter, G. Chudek, J.A., Houston, J.G., Belch, J.J.F., Non spiral and spiral (helical) flow patterns in stenoses - In vitro observations using spin and gradient echo magnetic resonance imaging (MRI) and computational fluid dynamics modeling, International Angiology, 23, 276-283, 2004.

11. Wilcox, D.C., Turbulence modelling for CFD, La Canada California: DWC Industries, 1993.

12. Ku, D.N., Blood flows in arteries, Annu. Rev. Fluid Mech., 29, 399-434, 1997.

13. FLUENT 6.3, Tutorials Guide. USA: Fluent INC, 2007.

14. Patankar, S.V., Spalding, D.B., A Calculation Procedure for Heat, Mass and Momentum Transfer in Three-dimensional Parabolic Flows, Int. J. Heat Mass Transfer, 15, 1787-1806, 1972.

15. Frydrychowicz, A., Harloff, A., Jung, B., Zaitsev, M., Eigang, E.W., Bley, T.A., Langer, M., Henning, J., Markl, M., Time-resolved, 3-dimensional magnetic resonance flow analysis at 3 T: visualization of normal and pathological aortic vascular hemodynamics, J. Comput. Assist. Tomogr., 31, 9-15, 2007.

16. Fry, D.L., Acute vascular endothelial changes associated with increased blood velocity gradients, Circulation Res., 22, 65–197, 1968.

	Ω (rad/sec)	
C	Re = 500	Re = 1000
0	0.0	0.0
$\dfrac{1}{12}$	0.73	1.46
$\dfrac{1}{6}$	1.46	2.92
$\dfrac{1}{4}$	2.19	4.38
$\dfrac{1}{3}$	2.92	5.84

Table 1: Spiral velocity (Ω) for the different values of C and Reynolds numbers.
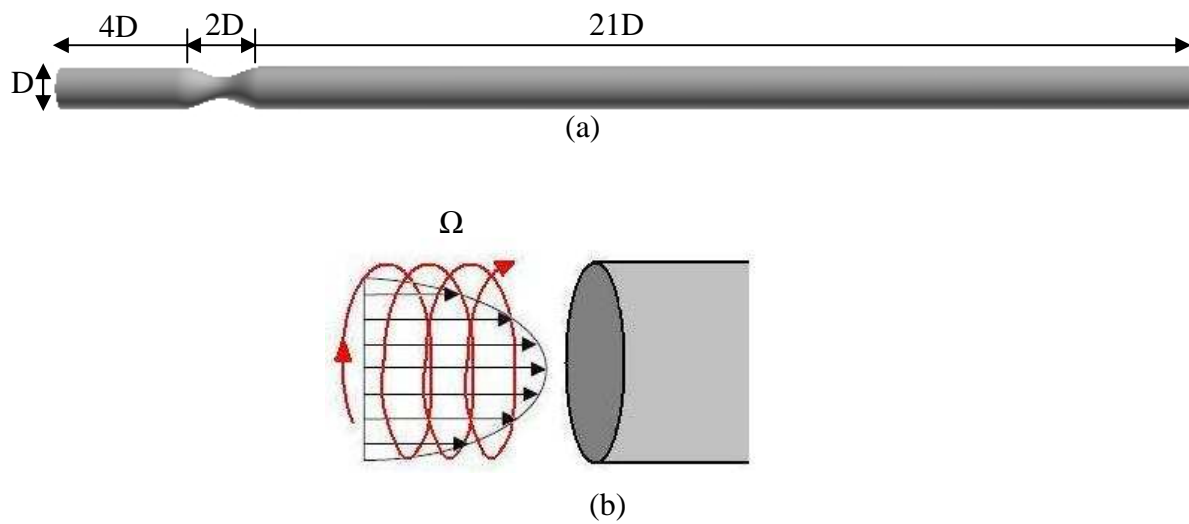
Figure 1: (a) Schematic of the model of a stenosed blood vessel and (b) An interpretation of the spiral boundary condition with the parabolic flow at the inlet of the model.
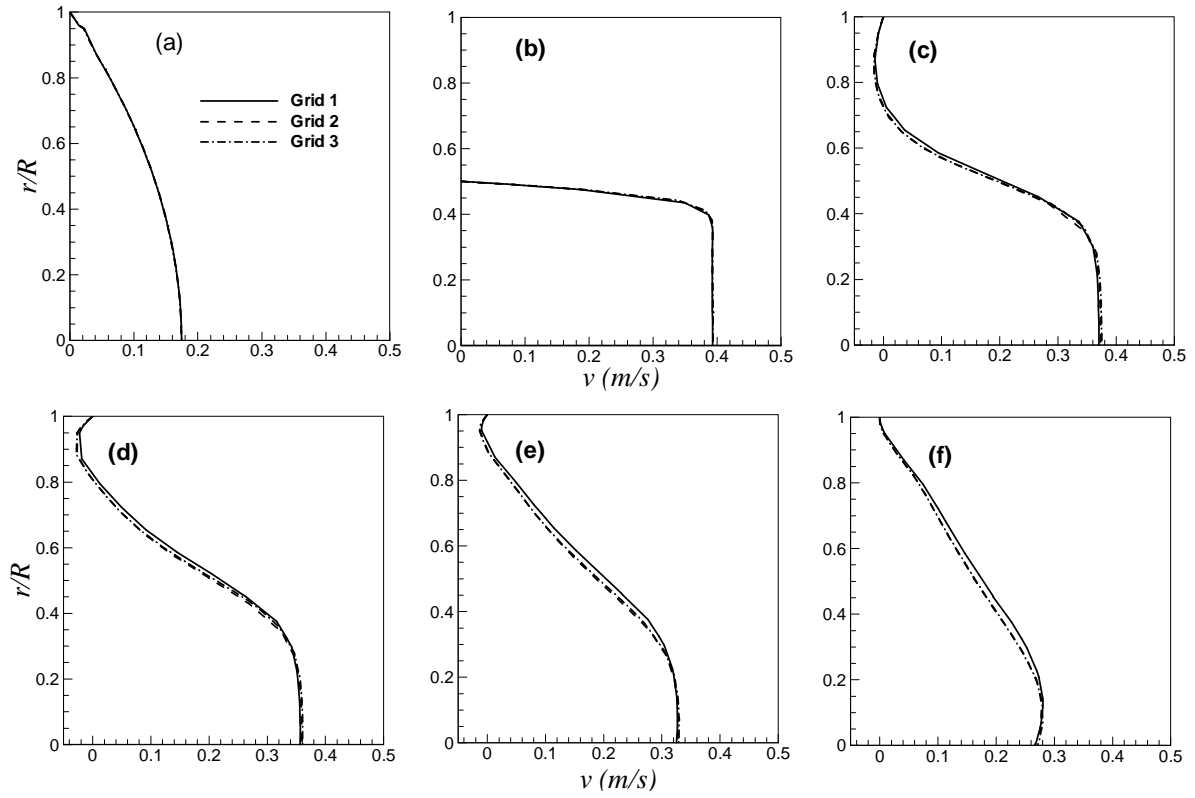
Figure 2: Grid independent test showing on the results of the axial velocity for Re=500 and Ω=1.46 rad/sec in (a) Z=-2D, (b) Z=0, (c) Z=1D, (d) Z=2D, (e) Z=3D and (f) Z=4D.
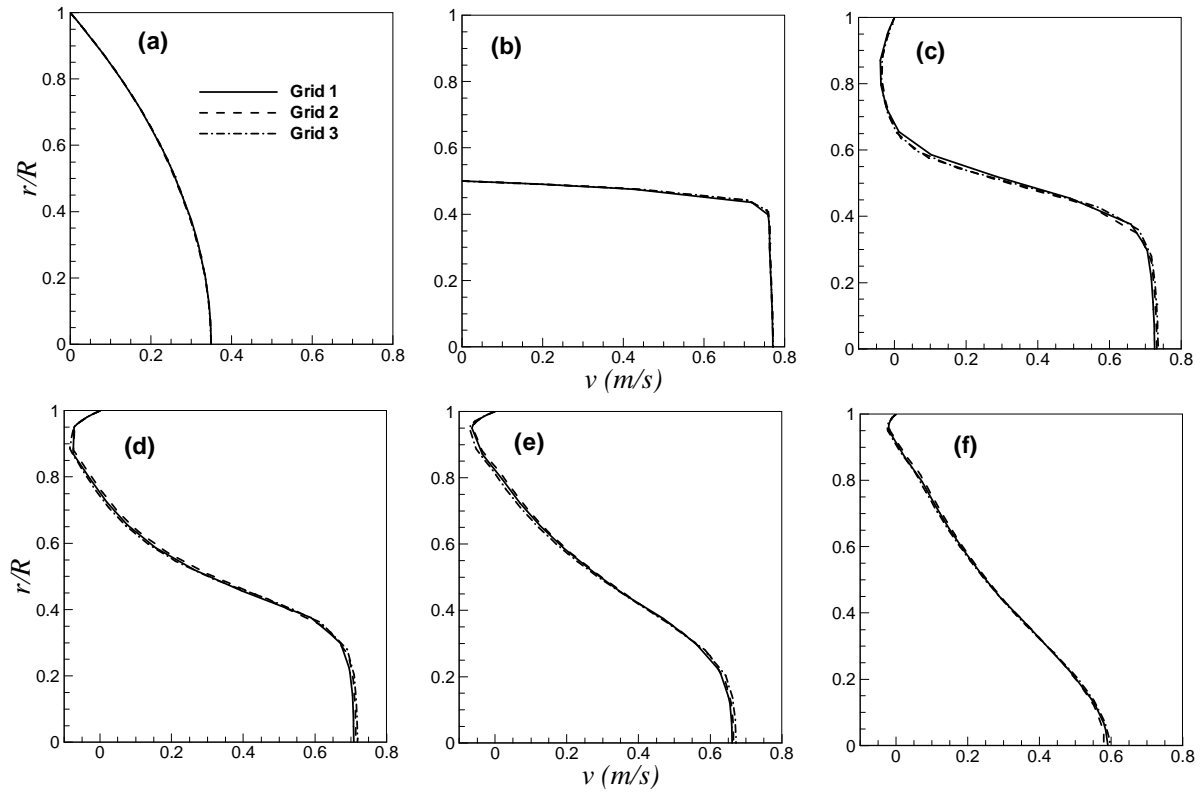
Figure 3: Grid independent test showing on the results of the axial velocity for Re=1000 and Ω=2.92 rad/sec in (a) Z=-2D, (b) Z=0, (c) Z=1D, (d) Z=2D, (e) Z=3D and (f) Z=4D.
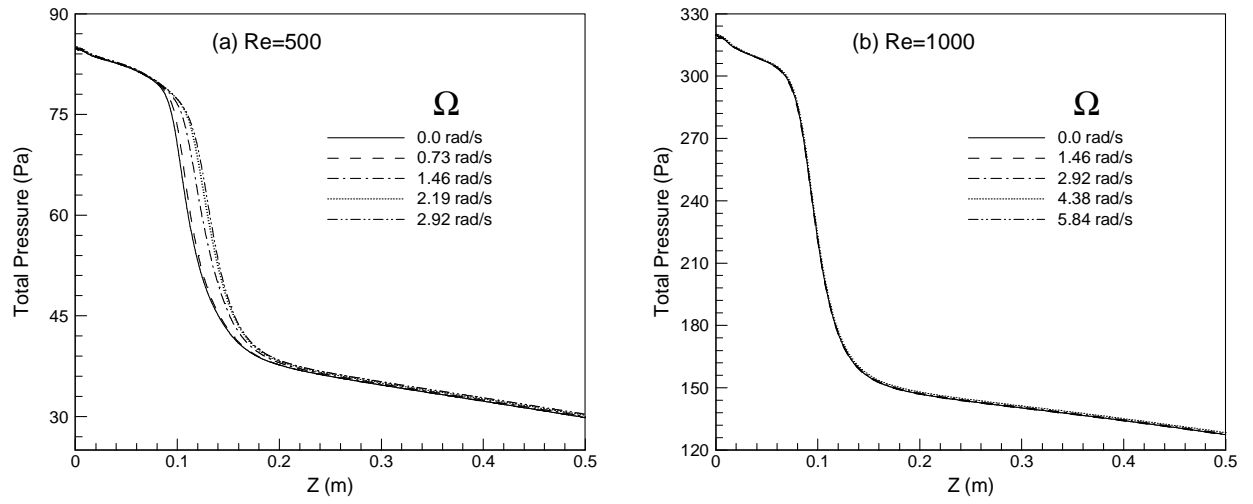
Figure 4: Centreline total pressure at various spiral speeds for (a) Re=500 and (b) Re=1000.
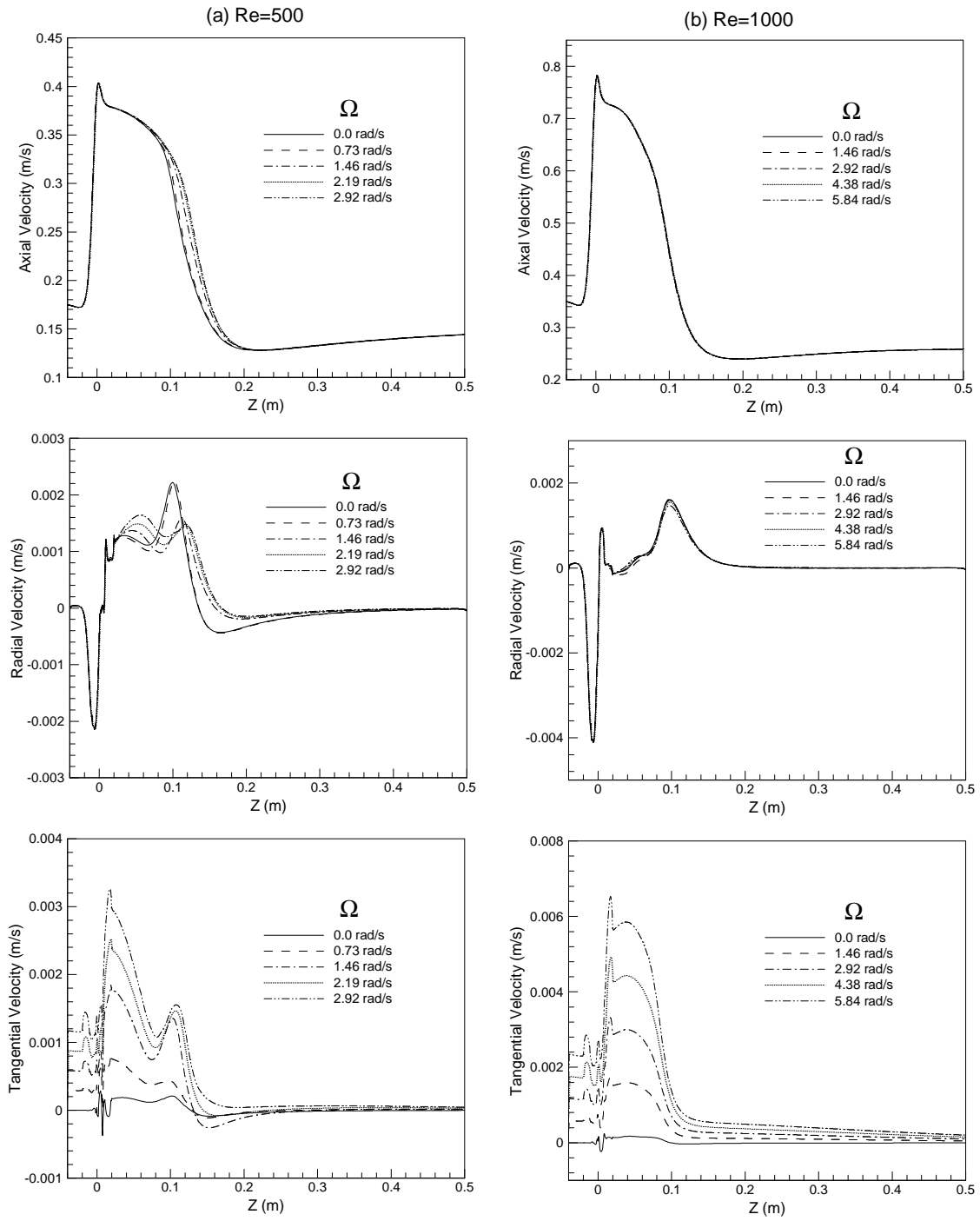
Figure 5: Centreline velocity at various spiral speeds for (a) Re=500 and (b) Re=1000.

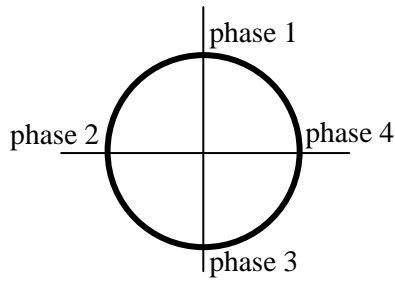(a) Re=500

0.0 rad/s

0.73 rad/s

1.46 rad/s

2.19 rad/s

2.92 rad/s

-0.0110   -0.0066   -0.0021   0.0023   0.0068   0.0112   0.0157   0.0201   0.0246   0.0290

(b) Re=1000

0.0 rad/s

1.46 rad/s

2.92 rad/s

4.38 rad/s

5.84 rad/s

-0.0200   -0.0111   -0.0022   0.0067   0.0156   0.0244   0.0333   0.0422   0.0511   0.0600
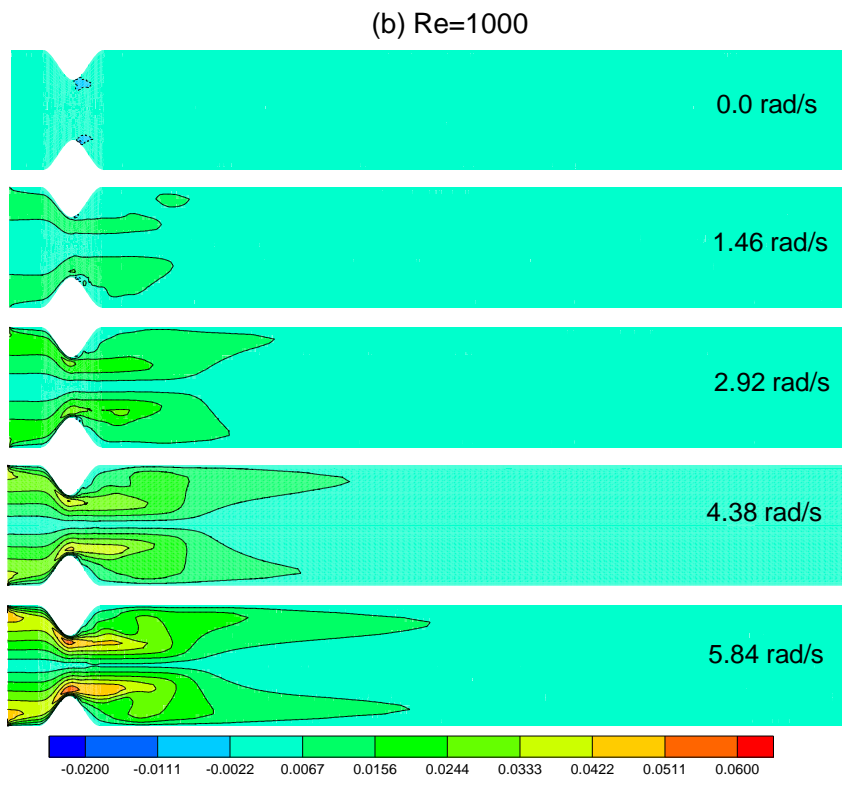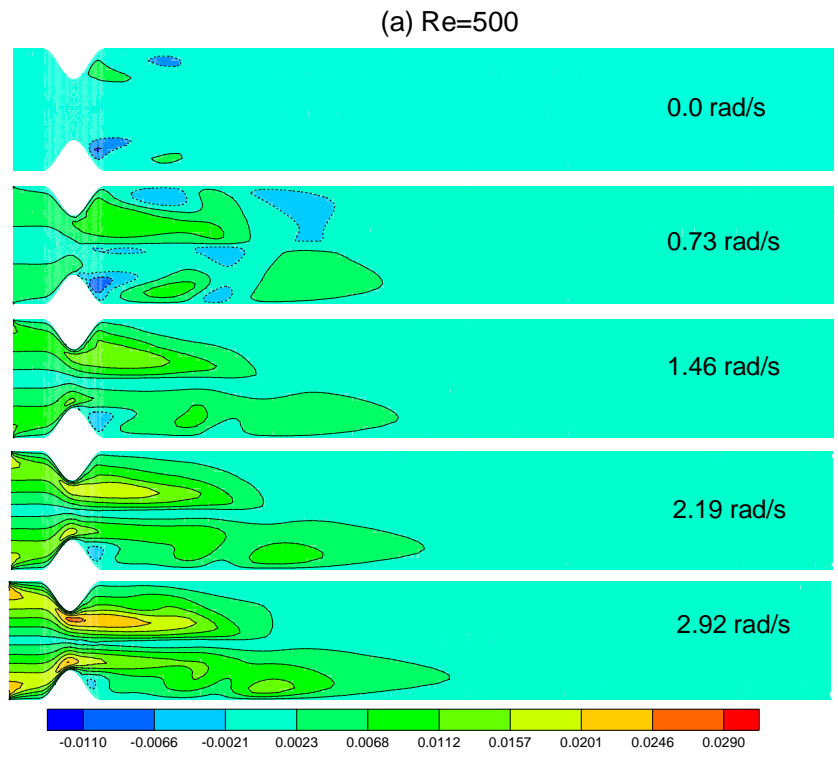
Figure 6: Tangential velocity at various spiral speeds for (a) Re=500 and (b) Re=1000.
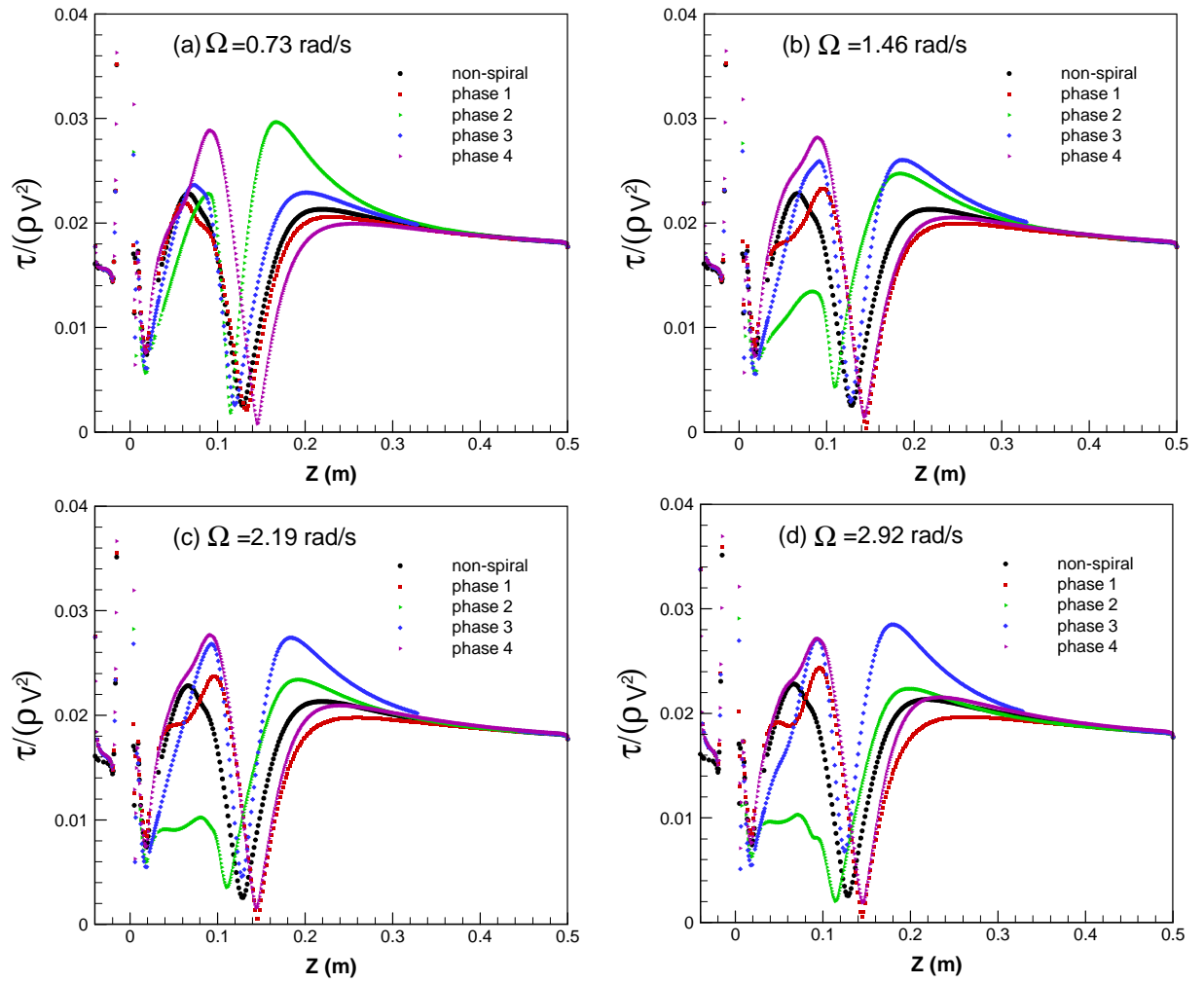
Figure 7: Wall shearing stress at different phases for Re=500 and different spiral speeds.
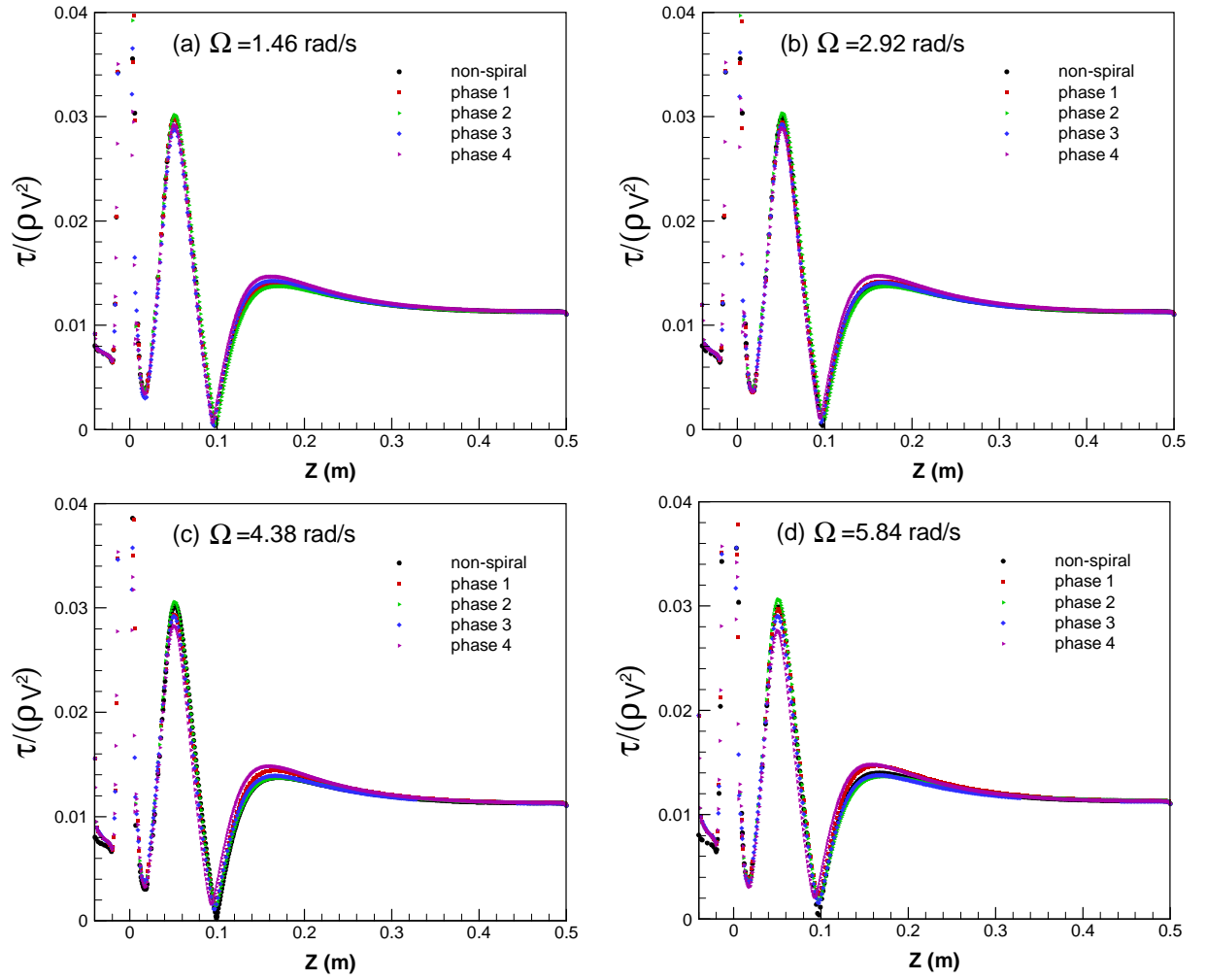
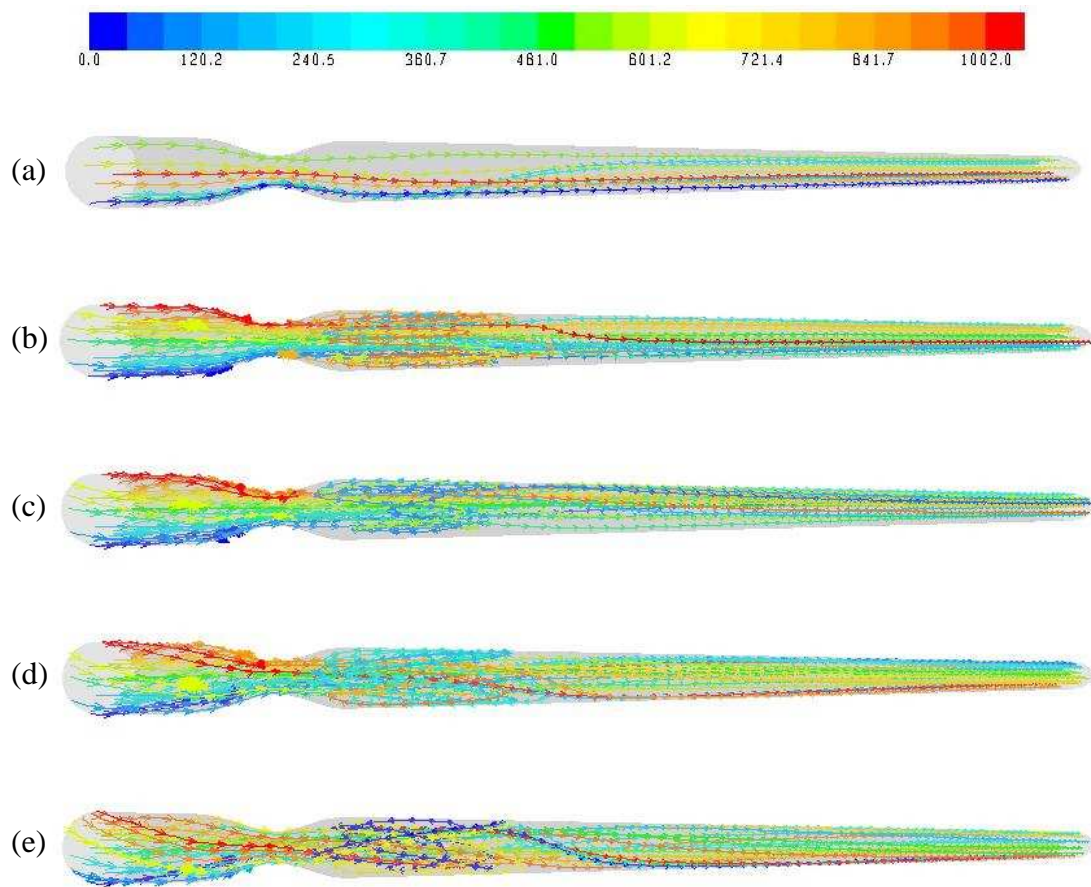Figure 8: Wall shearing stress at different phases for Re=1000 and different spiral speeds.

Figure 9: Pathlines, coloured by the particle ID, for Re=500 at different spiral speeds; (a) Ω=0.0 rad/s, (b) Ω=0.73 rad/s, (c) Ω=1.46 rad/s, (d) Ω=2.19 rad/s, and (e) Ω =2.92 rad/s.
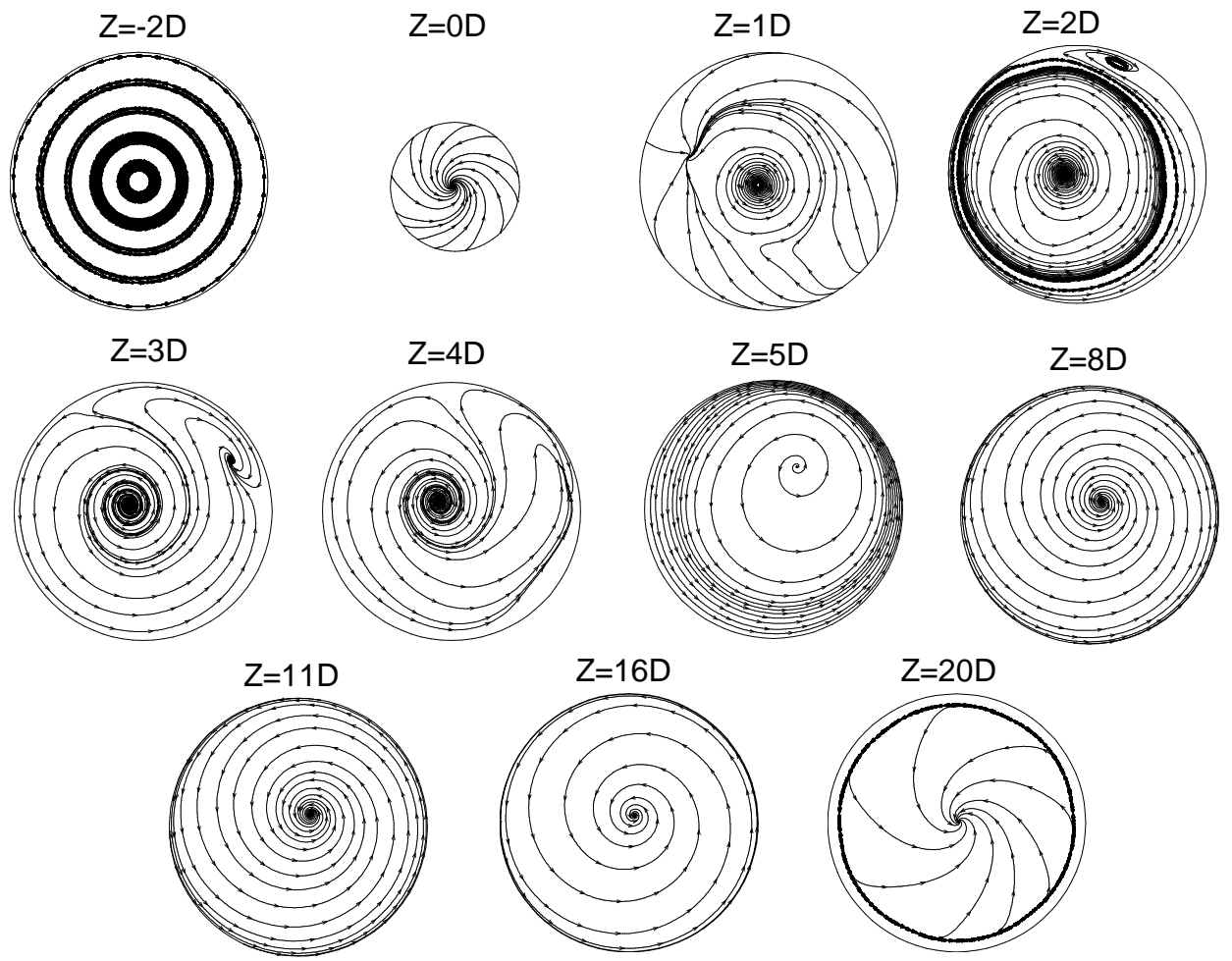
Figure 10: Streamlines at different axial positions for Ω=1.46 rad/s and Re=500.
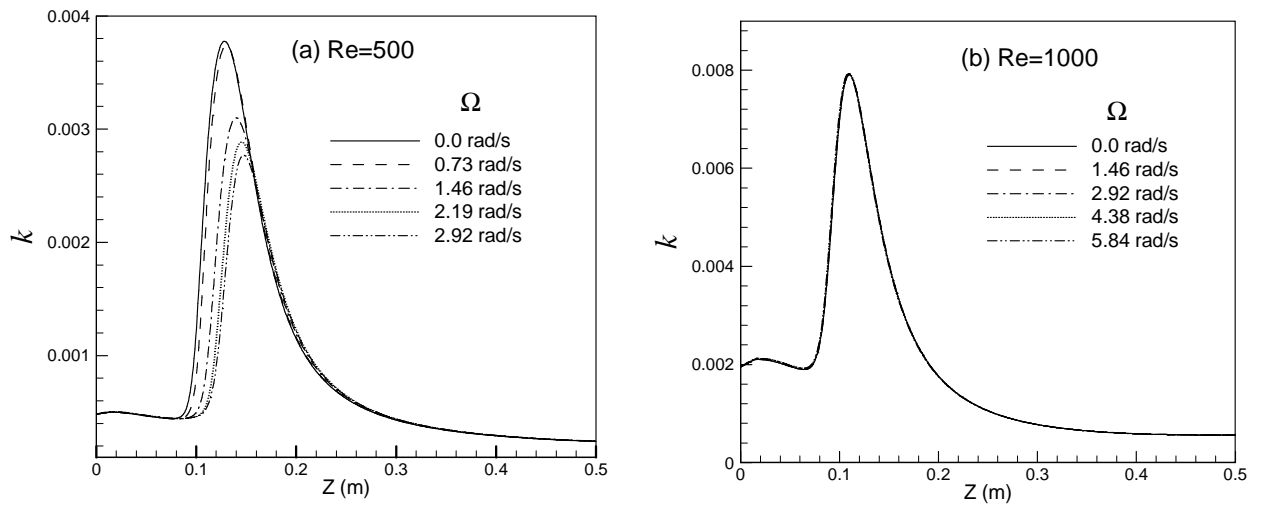
Figure 11: Turbulent kinetic energy (*k*) at different spiral speeds for (a) Re=500 and (b) Re=1000.